

Negative expansions of interatomic distances in metallic melts

Hongbo Lou^a, Xiaodong Wang^{a,1}, Qingping Cao^a, Dongxian Zhang^b, Jing Zhang^c, Tiandou Hu^c, Ho-kwang Mao^{a,d,e,1}, and Jian-Zhong Jiang^{a,f,1}

^aInternational Center for New-Structured Materials and Laboratory of New-Structured Materials, Department of Materials Science and Engineering, ^bState Key Laboratory of Modern Optical Instrumentation, and ^cState Key Laboratory of Silicon Materials, Zhejiang University, Hangzhou 310027, People's Republic of China; ^dBeijing Synchrotron Radiation Facility, Institute of High Energy Physics, Chinese Academy of Sciences, Beijing 100049, People's Republic of China; ^eCenter for High Pressure Science and Technology Advanced Research, Shanghai 201203, People's Republic of China; and ^fGeophysical Laboratory, Carnegie Institution of Washington, Washington, DC 20015

Contributed by Ho-kwang Mao, April 30, 2013 (sent for review April 2, 2013)

When a material is heated, generally, it dilates. Here, we find a general trend that the average distance between a center atom and atoms in the first nearest-neighbor shell contracts for several metallic melts upon heating. Using synchrotron X-ray diffraction technique and molecular dynamics simulations, we elucidate that this anomaly is caused by the redistribution of polyhedral clusters affected by temperature. In metallic melts, the high-coordinated polyhedra are inclined to evolve into low-coordinated ones with increasing temperature. As the coordination number decreases, the average atomic distance between a center atom and atoms in the first shell of polyhedral clusters is reduced. This phenomenon is a ubiquitous feature for metallic melts consisting of various-sized polyhedra. This finding sheds light on the understanding of atomic structures and thermal behavior of disordered materials and will trigger more experimental and theoretical studies of liquids, amorphous alloys, glasses, and casting temperature effect on solidification process of crystalline materials.

metal liquids | bond lengths | contraction

The study of metallic liquid structure is of importance because it is a fundamental issue in materials science and condensed-matter physics due to its critical role in understanding the processes of melting, solidification, and glass transition (1–6). Progress has been achieved in recent years both experimentally (7–24) and theoretically (13, 25–33). It is widely accepted that metallic liquids are composed of atomic clusters (7–33). However, how these clusters evolve upon external effects (e.g., temperature and pressure) still remains unclear (7–37). Generally, materials undergo thermal expansion and average atomic distance in the first shell increase upon heating. Here, we report a contraction of average atomic distance between a center atom and atoms in the first shell for metallic Al, Zn, Sn, In, Cu, Ni, Ag, and Au melts during heating. The thermal behaviors of metallic melts (pure elements and alloys) have been intensely studied, whereas the anomalous behavior of average atomic distance between a center atom and atoms in the first shell in liquids was usually ignored or not systematically evaluated (7–9, 21, 24). The anomalous behavior is focused upon and systematically investigated here by applying the state-of-the-art advanced synchrotron radiation-based experimental techniques and theoretical methods.

Results and Discussion

Fig. 1 shows the pair correlation function $g(r)$ at different temperatures for Al and Zn obtained by in situ high-temperature X-ray diffraction (XRD). Similar results for Sn and In metallic melts were also obtained in Fig. S1. The $g(r)$ was obtained by Fourier transformation of the structure factor $S(q)$ data, which reveals the average probabilities for finding atoms at a distance r for a given atom. In crystalline phases, atoms are located in discrete shells. However, in disordered structures they usually exhibit a broad distribution. The peak shape at various r values in $g(r)$ do not change obviously in the studied temperature range.

Fig. 1 *A* and *B* (*Inset*) is the local magnification of the first peak in $g(r)$. The reason to select the peak position is that at this distance the probability is the highest, which could be treated as an indicator for the change of atomic bonds. Upon heating, the peak positions in $g(r)$ shift. One striking observation is that the first peak positions in $g(r)$ move to low r rather than to large r values with increasing temperature for these single elements, e.g., 2.758 (1) Å at 937 K and 2.750(1) Å at 1077 K for Al, 2.645(1) Å at 710 K and 2.639(1) Å at 830 K for Zn, 3.104(1) Å at 543 K and 3.073 (1) Å at 1043 K for Sn, and 3.136(1) Å at 440 K and 3.098(1) Å at 890 K for In. Using the equation $\Delta l = (r_T - r_0)/r_0$, where r_0 and r_T denote the first peak position in $g(r)$ at the lowest studied temperature and at a given temperature T , the average bond length in the first shell decreased with a shrinkage rate of $1.87 \times 10^{-5} \text{ K}^{-1}$ for Al, $1.92 \times 10^{-5} \text{ K}^{-1}$ for Zn, $2.09 \times 10^{-5} \text{ K}^{-1}$ for Sn, and $2.78 \times 10^{-5} \text{ K}^{-1}$ for In in Fig. 1C. In addition, the real average distances that correspond to the “center of mass” of the first maximum in $g(r)$ as a function of temperature were calculated. The same decreasing trend is also revealed as in Fig. 1C. Peak positions from both pair distribution function (PDF) and radial distribution function [RDF = $4\pi r^2 g(r)$] for studied samples were also calculated (Fig. S2). They further confirm that the first peak position increases when temperature decreases, although the exact values deduced from PDF and RDF differ. The coordination number (CN) in the first shell is obtained by integrating the area of the first peak up to the first minimum. Using the equation $\Delta CN = (CN_T - CN_0)/CN_0$, a declining trend with the increasing temperature is clearly shown in Fig. 2, e.g., for Al 13.26(1) at 937 K and 13.12(1) at 1077 K, for Zn 13.01(1) at 710 K and 12.87(1) at 830 K, for Sn 10.33(1) at 543 K and 9.96(1) at 1043 K, and for In 11.13(1) at 440 K and 10.65(1) at 890 K. In general, it is difficult to define the nearest neighbors in liquids and determine a reliable CN. Different values in CN often occur when using different ways to estimate CN or using different cutoff distances. However, in the present work, the temperature dependences of CN are found to be the same when using different cutoff distances or using different ways (Fig. S3). To further confirm the contraction behavior of the average atomic bond length in the first shell for melts upon heating, we also carried out extended X-ray absorption fine-structure (EXAFS) measurements at the Zn *K* edge at three different temperatures for liquid Zn in Fig. 3. A single-distance shell model was used to simulate the EXAFS results. A good agreement between the

Author contributions: J.-Z.J. designed research; H.L., X.W., D.Z., J.Z., and T.H. performed research; H.L., X.W., Q.C., H.-k.M., and J.-Z.J. analyzed data; and X.W. and J.-Z.J. wrote the paper.

The authors declare no conflict of interest.

¹To whom correspondence may be addressed. E-mail: jiangjz@zju.edu.cn, wangxd@zju.edu.cn, or mao@gl.ciw.edu.

This article contains supporting information online at www.pnas.org/lookup/suppl/doi:10.1073/pnas.1307967110/-DCSupplemental.

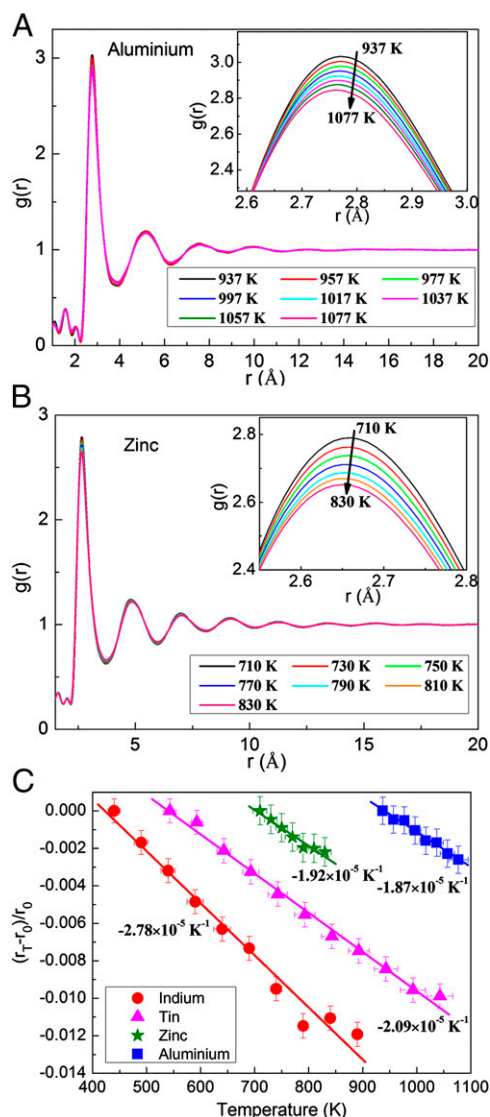


Fig. 1. First peak position of $g(r)$ curves shift upon heating for liquid melts. (A) $g(r)$ curves for Al with temperature increasing from 937 to 1077 K with 20-K increment. (B) $g(r)$ curves for Zn with temperature increasing from 710 to 830 K with 20-K increment. (A and B, Insets) Local magnification of the top part for the first peak of $g(r)$, showing the reduced peak intensity and peak positions shift to low r values with increasing temperature. (C) Variation of the first peak position in $g(r)$ changing with temperature for metallic Al, Zn, Sn, and In melts. The lines are the linear fit of the peak position.

simulated result and the experimental one is shown in Fig. 3A, *Inset*. It is found that the average bond length in the first shell indeed decreases with increasing temperature in Fig. 3B. Results obtained both from in situ XRD and in situ EXAFS measurements reveal that the average bond length between center atom and atoms in the first shell does contract with increasing temperature in studied metallic melts.

Molecular dynamics (MD) simulation plays an important role in understanding the atomic structure and the related properties of complex systems. To uncover the mechanism for the finding mentioned above, MD simulations were performed for the selected single elements of Al, Cu, Ag, Au, and Ni, by which good reliable atomic potentials are available (38–40). Agreements in $g(r)$ and $S(q)$ between the MD simulated data and experimental ones (Fig. S4) were achieved for Al. Fig. 4A shows the $g(r)$ of pure Al changing with temperature from 400 to 2000 K produced by

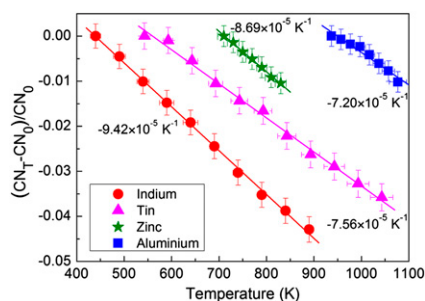


Fig. 2. Variation of CN for the first shell changing with temperature for metallic Al, Zn, Sn, and In melts. The lines are the linear fit of CN.

MD. The melting point is at the temperature between about 900 and 1000 K, which is close to the experimental value of 933.5 K. It is demonstrated that the peak intensity is significantly reduced and the first peak position in $g(r)$ indeed shifts to low r values after melting upon heating, which is consistent with the experimental observations in Fig. 1. Using the Voronoi tessellation

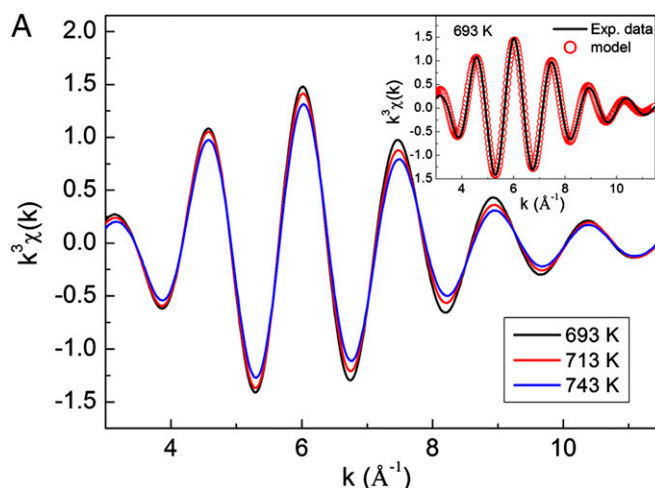


Fig. 3. Structural changes in liquid Zn with increasing temperature by EXAFS experiments. (A) Backward Fourier transform results obtained from in situ EXAFS experiments of liquid Zn at three different temperatures: 693, 713, and 743 K. (*Inset*) Comparison of the simulated results and the experimental one at 693 K. (B) Declining trend for the bond length estimated from the single-distance shell model simulation at three temperatures. The line is the linear fit of the three points.

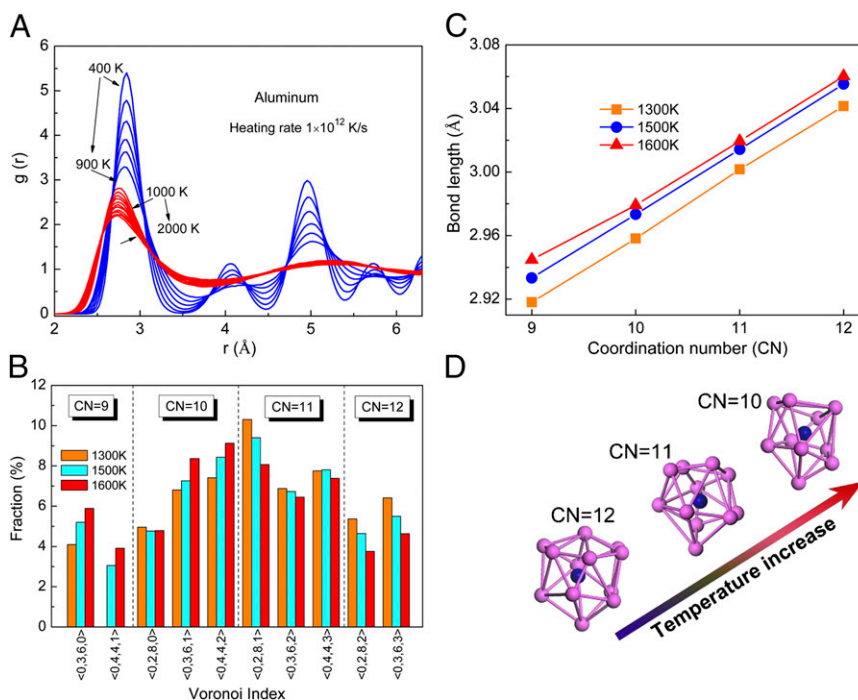


Fig. 4. Structural changes in liquid Al with increasing temperature reproduced by MD simulation. (A) $g(r)$ curves for Al heated from 400 to 2,000 K indicate the melting point at a temperature between 900 and 1,000 K. (B) Fractions of polyhedra at different temperatures; those higher than 3% are shown. Upon heating, the number of high-coordinated polyhedra is reduced with the low-coordinated uprising. (C) Relationship between the average bond length between center atom and atoms in the first shell and CN value, showing the bond length of high-coordinated polyhedra is larger than that of low-coordinated ones, whereas in the polyhedra with the same CN values the bond length still expands with increasing temperature. (D) Schematically shows the evolution from high-coordinated to low-coordinated polyhedra with temperature increase. The increased weight factor of low-coordinated polyhedra leads to the reduced bond length between center atom and atoms in the first shell.

method (41) with a cutoff of 3.7 \AA , the evolution of polyhedra within the nearest neighbor was studied for Al melts. The fraction of ideal icosahedron of $\langle 0,0,12,0 \rangle$ is quite low (about 1%), and Fig. 4B displays that most icosahedron-like polyhedra are $\langle 0,2,8,0 \rangle$, $\langle 0,2,8,1 \rangle$, and $\langle 0,2,8,2 \rangle$. With increasing temperature, the tendency of atomic configuration evolution is that the fractions of high-coordinated polyhedra like 11- and 12-coordinated are decreased. Accordingly, low-coordinated polyhedra (9- and 10-coordinated) are distinctly increased. This implies that high-coordinated polyhedra are relatively stable at low temperatures, and vice versa. Fig. 4C shows that the average bond lengths between center atom and atoms in the first shell change with the CN, indicating that high-coordinated polyhedra have larger average distances between center atom and atoms in the shell than those of low-coordinated ones. Bond lengths in polyhedra having the same CN value increase at high temperatures. Usually, the larger the distance between atoms, the weaker the bonding will be. High temperature makes atoms vibrate drastically, which could drive some of them to break away from high-coordinated polyhedra where the weaker atomic bonds are located. Consequently, it is an intrinsic nature that the polyhedra in metallic melts become low-coordinated clusters with short bond lengths at higher temperatures. Fig. 4D schematically shows that the major polyhedra change from CN = 12 to CN = 10 with temperature increase. Indeed, the similar variation tendency was observed for single elements of Cu, Au, Ag, and Ni (details shown in Figs. S5–S8). Fig. 5A clearly reveals negative variations of average bond length between center atom and atoms in the first shell as a function of temperature for Al, Cu, Ag, Au, and Ni liquids with increasing temperature from MD simulations. The similar trend in the coordinate number reduction is displayed in Fig. 5B, in good agreement with the above experimental results for

Al, Zn, Sn, and In. All results obtained for liquid zinc from ab initio MD simulation and reverse Monte Carlo simulation in Figs. S9 and S10 are also consistent with the results mentioned above.

The finding mentioned above could be a ubiquitous phenomenon for metallic melts upon heating. The origination of this phenomenon comes from the structural change in the first shell, that is, the number of high-coordinated polyhedra, in which atoms have large average atomic distance between a center atom and atoms in the shell, is reduced when temperature increases, forming more close-packed small clusters. Consequently, the average atomic distance and CN in the first shell decreases with increasing temperature. However, on the macroscopic scale, the bulk volume of liquids is expanded as shown in Fig. S11. The average bond lengths for the high-order shells (>2) in $g(r)$ indeed gradually increase with temperature in most studied liquids in Figs. S12 and S13. Hence, most likely, more excess open volumes (or free volumes) are created between polyhedra, thereby reducing the liquid density upon heating (42, 43). In addition, although the shift of the first peak to lower r values in $g(r)$ was reported for multicomponent alloys (21, 44, 45) and some speculations were stated in the previous published papers (7–9, 24), it is still impossible to deduce the atomic bond change due to the overlapping effect of many atomic bonds in multicomponent alloy systems, e.g., 3 atomic bonds (A–A, A–B, and B–B pairs) for a binary alloy A–B system and 10 atomic bonds (A–A, A–B, A–C, A–D, B–B, B–C, B–D, C–C, C–D, and D–D pairs) for a quaternary alloy A–B–C–D system. Only using simple pure metal elements, the atomic distance in the first shell can be unambiguously determined from the first peak shift in pair correlation function. Moreover, a liquid can be transformed into a glass upon cooling if the crystallization is bypassed. Our results that at high temperatures the melts contain many low-coordinated

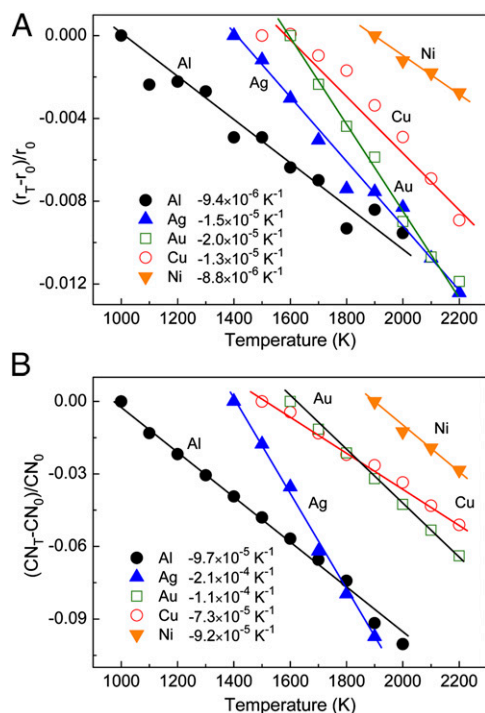


Fig. 5. MD simulated structural changes for liquid Al, Cu, Ag, Au, and Ni. (A) Bond length and (B) CN altered with temperature increase. Almost the same variation trends are present, quite consistent with above experimental results for Al.

polyhedral, whereas at low temperatures they have high-coordinated polyhedra of icosahedron-like clusters, can explain that reported experimental results, e.g., different temperatures of melts, at which melts are quenched, could affect the glass-forming process, thermal stability, and mechanical properties of systems (46–52). Furthermore, our finding might also shed light on the casting temperature effect on solidification process in crystalline systems, and the glass transition phenomenon in disordered systems because they are atomic packing related as well.

Conclusions

In summary, the atomic structure changes of liquid Al, Zn, Sn and In upon heating have been measured by in situ synchrotron X-ray diffraction and/or EXAFS, and those of liquid Al, Cu, Ag, Au, and Ni reproduced by classic MD simulations and Zn by ab initio MD simulations. We proposed a scenario describing metallic clusters evolution in the liquid state, i.e., high-coordinated clusters with larger bond length between a center atom and atoms in the shell declined into low-coordinated clusters with smaller bond length upon heating. We observed the contraction

of average atomic distance between a center atom and atoms in the first shell and the reduction in CN in the first shell for eight metallic melts upon heating. Such structural evolution can further promote the understanding of thermal behavior of disordered materials including melting, solidification, glass transition, and phase transition in liquid phases.

Methods

The high-energy XRD measurements were carried out on the BW5 station by using synchrotron radiation with a wavelength of 0.124 Å at HASYLAB/DESY, Hamburg. Pure Al, Zn, Sn, and In wire were cut into fine pieces and then transferred into a capillary 2 mm in diameter. After pumping, a vacuum environment in the capillary was created. The heater is composed of twin face-to-face tungsten bulbs. The furnace temperature was calibrated and controlled by two thermocouples, one inside the capillary reaching a place just above the sample, and another in the chamber. The X-ray beam size and wavelength used were $0.5 \times 0.5 \text{ mm}^2$ and 0.124 Å, respectively. Upon heating, the diffraction patterns were in situ automatically collected from 323 K by a flat-panel Si detector (Perkin-Elmer 1621) with $200 \times 200 \mu\text{m}^2$ pixel size and 2048×2048 pixels. Exposure time was 2 s, and five diffraction patterns were summed for each data set. Scattering intensity $I(q)$ (vs. scattering vector) were extracted by using the software package FIT2D (53). From $I(q)$, structure factor $S(q)$ and PDF $G(r)$ could be obtained by using the program PDFgetX2 (54). Then, the pair correlation function $g(r)$ is calculated by $g(r) = 1 + G(r)/4\pi r \rho_0$, where ρ_0 is the atomic number density. For Zn melts, high-temperature EXAFS measurements (55) at the Zn K edge on the beamline 1W1B-XAFS of the Beijing Synchrotron Radiation Facility were also carried out because this technique can give the average atomic bond length in the first shell, whereas a detailed description can be found in *SI Methods*.

Molecular dynamics (MD) simulations were performed for the selected single elements of Al, Cu, Ag, Au, and Ni. Adopting well-developed embedded atom method potentials for such elements (38–40), we simulated the whole thermal process by using the LAMMPS code (56). A cubic box containing 20,000 atoms with 3D periodic boundary conditions was heated to about 800 K above their melting points under zero external pressure (constant number of particles, constant pressure, and constant temperature ensembles and Nosé–Hoover thermostat) (57) at a heating rate of $1 \times 10^{12} \text{ K/s}$. Lacking a good atomic potential for Zn, ab initio MD simulations for 128 Zn atoms were also carried out by using the density functional theory implemented in the Vienna ab initio simulation package (VASP) code (58). Detailed description of the ab initio MD simulation and reverse Monte Carlo simulation for pure Zn is given in *SI Methods*.

ACKNOWLEDGMENTS. The authors thank the HASYLAB staff of BW5 for assistance during the XRD measurements and the Beijing Synchrotron Radiation Facility staff of 1W1B-XAFS for the EXAFS measurements. Financial support was received from the National Key Basic Research Program of China (2012CB825700), National Natural Science Foundation of China (Grants 10979002, 50920105101, 51071141, 51050110136, 11179026, and 10904127), Natural Science Foundation of Zhejiang Province (Z1110196), and the Zhejiang University–Helmholtz Cooperation Fund (IK Ch-0002). The authors also acknowledge fundamental research funds for the central universities and the Department of Science and Technology of Zhejiang Province and Zhejiang University and the Shanghai Supercomputer Center for supporting the MD simulations with the magic supercomputer. H.-k.M. was supported as part of EFree, an Energy Frontier Research Center funded by the US Department of Energy, Office of Science, Office of Basic Energy Sciences under Award DE-SC0001057.

- Nelson DR (1983) Order, frustration, and defects in liquids and glasses. *Phys Rev B* 28(10):5515–5535.
- Debenedetti PG, Stillinger FH (2001) Supercooled liquids and the glass transition. *Nature* 410(6825):259–267.
- Reichert H, et al. (2000) Observation of five-fold local symmetry in liquid lead. *Nature* 408(6814):839–841.
- Siwick BJ, Dwyer JR, Jordan RE, Miller RJD (2003) An atomic-level view of melting using femtosecond electron diffraction. *Science* 302(5649):1382–1385.
- Asta M, et al. (2009) Solidification microstructures and solid-state parallels: Recent developments, future directions. *Acta Mater* 57(4):941–971.
- Jin ZH, Gumbsch P, Lu K, Ma E (2001) Melting mechanisms at the limit of superheating. *Phys Rev Lett* 87(5):055703.
- Schenk T, Holland-Moritz D, Simonet V, Bellissent R, Herlach DM (2002) Icosahedral short-range order in deeply undercooled metallic melts. *Phys Rev Lett* 89(7):075507.
- Holland-Moritz D, et al. (2002) Short-range order in undercooled Co melts. *J Non-Cryst Solids* 312–314:47–51.
- Itami T, et al. (2003) Structure of liquid Sn over a wide temperature range from neutron scattering experiments and first-principles molecular dynamics simulation: A comparison to liquid Pb. *Phys Rev B* 67(6):064201.
- Kelton KF, et al. (2003) First x-ray scattering studies on electrostatically levitated metallic liquids: Demonstrated influence of local icosahedral order on the nucleation barrier. *Phys Rev Lett* 90(19):195504.
- Lee GW, et al. (2004) Difference in icosahedral short-range order in early and late transition metal liquids. *Phys Rev Lett* 93(3):037802.
- Kim TH, et al. (2005) In situ high-energy x-ray diffraction study of the local structure of supercooled liquid Si. *Phys Rev Lett* 95(8):085501.
- Ganesh P, Widom M (2006) Signature of nearly icosahedral structures in liquid and supercooled liquid copper. *Phys Rev B* 74(13):134205.
- Kim TH, Kelton KF (2007) Structural study of supercooled liquid transition metals. *J Chem Phys* 126(5):054513.
- Holland-Moritz D, Heinen O, Bellissent R, Schenk T (2007) Short-range order of stable and undercooled liquid titanium. *Mater Sci Eng A* 449:42–45.

16. Shen YT, Kim TH, Gangopadhyay AK, Kelton KF (2009) Icosahedral order, frustration, and the glass transition: Evidence from time-dependent nucleation and supercooled liquid structure studies. *Phys Rev Lett* 102(5):057801.
17. Liu XJ, et al. (2010) Metallic liquids and glasses: Atomic order and global packing. *Phys Rev Lett* 105(15):155501.
18. Beye M, Sorgenfrei F, Schlotter WF, Wurth W, Föhlisch A (2010) The liquid-liquid phase transition in silicon revealed by snapshots of valence electrons. *Proc Natl Acad Sci USA* 107(39):16772–16776.
19. Mauro NA, et al. (2011) Short- and medium-range order in Zr₈₀Pt₂₀ liquids. *Phys Rev B* 83(18):184109.
20. Mauro NA, Bendert JC, Vogt AJ, Gewin JM, Kelton KF (2011) High energy x-ray scattering studies of the local order in liquid Al. *J Chem Phys* 135(4):044502.
21. Georganakis K, et al. (2011) Variations in atomic structural features of a supercooled Pd-Ni-Cu-P glass forming liquid during in situ vitrification. *Acta Mater* 59(2):708–716.
22. Chirawatkul P, et al. (2011) Structure of eutectic liquids in the Au-Si, Au-Ge, and Ag-Ge binary systems by neutron diffraction. *Phys Rev B* 83(1):014203.
23. Kang JG, Zhu JY, Wei SH, Schwegler E, Kim YH (2012) Persistent medium-range order and anomalous liquid properties of Al_(1-x)Cu_(x) alloys. *Phys Rev Lett* 108(11):115901.
24. Mauro NA, et al. (2012) Local atomic structure in equilibrium and supercooled liquid Zr_(75.5)Pd_(24.5). *J Chem Phys* 137(4):044501.
25. Jakse N, Pasturel A (2003) Local order of liquid and supercooled zirconium by ab initio molecular dynamics. *Phys Rev Lett* 91(19):195501.
26. Jakse N, Pasturel A (2004) Ab initio molecular dynamics simulations of local structure of supercooled Ni. *J Chem Phys* 120(13):6124–6127.
27. Ganesh P, Widom M (2008) Ab initio simulations of geometrical frustration in supercooled liquid Fe and Fe-based metallic glass. *Phys Rev B* 77(1):134205.
28. Becker CA, Kramer MJ (2010) Atomistic comparison of volume-dependent melt properties from four models of aluminum. *Model Simul Mater Sci* 18(7):074001.
29. Huang L, Wang CZ, Ho KM (2011) Structure and dynamics of liquid Ni₃₆Zr₆₄ by ab initio molecular dynamics. *Phys Rev B* 83(18):184103.
30. Wu S, et al. (2011) Structural and dynamical properties of liquid Cu₉₀Si₁₀ alloy studied experimentally and by ab initio molecular dynamics simulations. *Phys Rev B* 84(13):134208.
31. Vasisht VV, Saw S, Sastry S (2011) Liquid-liquid critical point in supercooled silicon. *Nat Phys* 7(7):549–553.
32. Thakor PB, Sonvane YA, Jani AR (2011) Structural properties of some liquid transition metals. *Phys Chem Liq* 49(4):530–549.
33. Egami T (2007) Icosahedral order in liquids. *J Non-Cryst Solids* 353(32–40):3666–3670.
34. Narushima T, Hattori T, Kinoshita T, Hinzmann A, Tsuji K (2007) Pressure dependence of the structure of liquid Sn up to 19.4 GPa. *Phys Rev B* 76(10):104204.
35. Iwashita T, Egami T (2012) Atomic mechanism of flow in simple liquids under shear. *Phys Rev Lett* 108(19):196001.
36. Yang JJ, Tse JS, Iitaka T (2011) First-principles study of liquid gallium at ambient and high pressure. *J Chem Phys* 135(4):044507.
37. Shen GY, Prakash VB, Rivers ML, Sutton SR (2004) Structure of liquid iron at pressures up to 58 GPa. *Phys Rev Lett* 92(18):185701.
38. Foiles SM, Baskes MI, Daw MS (1986) Embedded-atom-method functions for the fcc metals Cu, Ag, Au, Ni, Pd, Pt, and their alloys. *Phys Rev B Condens Matter* 33(12):7983–7991.
39. Zhou XW, Johnson RA, Wadley HNG (2004) Misfit-energy-increasing dislocations in vapor-deposited CoFe/NiFe multilayers. *Phys Rev B* 69(14):144113.
40. Sheng HW, Kramer MJ, Cadien A, Fujita T, Chen MW (2011) Highly optimized embedded-atom-method potentials for fourteen fcc metals. *Phys Rev B* 83(13):134118.
41. Finney JL (1977) Modeling structures of amorphous metals and alloys. *Nature* 266(5600):309–314.
42. Wang LW, Wang Q, Xian AP, Lu KQ (2003) Precise measurement of the densities of liquid Bi, Sn, Pb and Sb. *J Phys Condens Matter* 15(6):777–783.
43. Wang LW, Mei QS (2006) Density measurement of liquid metals using dilatometer. *J Mater Sci Technol* 22(4):569–571.
44. Mattern N, et al. (2003) Structural behavior of Pd₄₀Cu₃₀Ni₁₀P₂₀ bulk metallic glass below and above the glass transition. *Appl Phys Lett* 82(16):2589–2591.
45. Jiang QK, Chang ZY, Wang XD, Jiang JZ (2010) Structures at glassy, supercooled liquid, and liquid states in La-based bulk metallic glasses. *Metall Mater Trans, A Phys Metall Mater Sci* 41A(7):1634–1639.
46. Mukherjee S, Zhou Z, Schroers J, Johnson WL, Rhim WK (2004) Overheating threshold and its effect on time-temperature-transformation diagrams of zirconium based bulk metallic glasses. *Appl Phys Lett* 84(24):5010–5012.
47. Way C, Wadhwa P, Busch R (2007) The influence of shear rate and temperature on the viscosity and fragility of the Zr_{41.2}Ti_{13.8}Cu_{12.5}Ni_{10.0}Be_{22.5} metallic-glass-forming liquid. *Acta Mater* 55(9):2977–2983.
48. Mao J, et al. (2009) The effects of casting temperature on the glass formation of Zr-based metallic glasses. *Adv Eng Mater* 11(12):986–991.
49. Kumar G, Ohkubo T, Hono K (2009) Effect of melt temperature on the mechanical properties of bulk metallic glasses. *J Mater Res* 24(7):2353–2360.
50. Hu Y, Li JF, Lin T, Zhou YH (2009) Plasticity improvement of Zr₅₅Al₁₀Ni₅Cu₃₀ bulk metallic glass by remelting master alloy ingots. *J Mater Res* 24(12):3590–3595.
51. Schroers J (2010) Processing of bulk metallic glass. *Adv Mater* 22(14):1566–1597.
52. Mu JA, et al. (2010) The effect of melt treatment on glass forming ability and thermal stability of Al-based amorphous alloy. *Adv Eng Mater* 12(11):1127–1130.
53. Hammersley AP, Svensson SO, Hanfland M, Fitch AN, Hausermann D (1996) Two-dimensional detector software: From real detector to idealised image or two-theta scan. *High Press Res* 14(4–6):235–248.
54. Qiu X, Thompson JW, Billinge SJL (2004) PDFgetX2: A GUI-driven program to obtain the pair distribution function from X-ray powder diffraction data. *J Appl Cryst* 37:678.
55. Pettifer RF, Mathon O, Pascarelli S, Cooke MD, Gibbs MRJ (2005) Measurement of femtometre-scale atomic displacements by X-ray absorption spectroscopy. *Nature* 435(7038):78–81.
56. Plimpton S (1995) Fast parallel algorithms for short-range molecular-dynamics. *J Comput Phys* 117(1):1–19.
57. Nose S (1984) A unified formulation of the constant temperature molecular-dynamics methods. *J Chem Phys* 81(1):511–519.
58. Kresse G, Furthmüller J (1996) Efficiency of ab-initio total energy calculations for metals and semiconductors using a plane-wave basis set. *Comput Mater Sci* 6(1):15–50.